Asian Journal of Chemistry; Vol. 31, No. 1 (2019), 83-88

ASIAN JOURNAL OF CHEMISTRY

https://doi.org/10.14233/ajchem.2019.21546

Preparation and Characterization of Ball Clay-Manganese Dioxide Nanocomposites

K. THIRUMOORTHY* and S.K. KRISHNA

Department of Chemistry, Chikkaiah Naicker College, Erode-638004, India

*Corresponding author: E-mail: kthiru86@gmail.com

Received: 27 June 2018; *Accepted*: 14 August 2018; *Published online*: 30 November 2018; AJC-19163

We report in present work the simple procedure to synthesize ball clay-manganese dioxide (MnO_2) nanocomposites. The as-synthesized nanocomposites were characterized using powder XRD, FT-IR, SEM, TEM and BET surface area, respectively. Recently the explorations of clay modification for developing the adsorbent ability to get rid of the toxins from water. The XRD result indicates that the nanocomposite was crystalline in nature. The FTIR spectra showed that the native ball clay was successfully converted to ball clay-MnO_2 nanocomposites, which were identified by the change in peaks. The SEM images of the ball clay-MnO_2 nanocomposites showed that development in surface area. The TEM images indicated that the size of the nanoparticle. The BET studies of as synthesized ball clay-MnO_2 nanocomposites indicate that surface area, total pore volume and average pore diameter values.

Keywords: Ball clay, Manganese dioxide, Adsorbent, Nanocomposite.

INTRODUCTION

The main problem of the textile industries are releasing the massive amount of dyes in river or other water system. Owing to this badly behaviour results in contamination of underground water and damaging the entire ecological system. The main challenge is treatment of the polluted water without damage of environment. Over the past years, numerous techniques for the treatment of textile wastewater including of membrane filtration [1], ozonation [2], biosorption [3], electro coagulation [4], photo catalytic removal [5], coagulation and flocculation [6], electrochemical precipitation [7]. Nevertheless, these methods having some inadequacy to remove the dyes from wastewater.

Nowadays, adsorption technique is a well-known method for the treatment of wastewater from dyes and heavy metals. At present, adsorption techniques have been considered owing to the low cost, ease of operation and less amount of residue. The dyes can be efficiently removed by adsorption technique in, which the liquefied dyes attached themselves to the adsorbent surface. Several adsorbents have been used for removal of dyes from aqueous solution. The adsorbents such as recycled alum sludge [8], waste coir pith [9], fir wood [10], rotton saw dust [11], fly ash [12], coconut shells [13], activated carbon [14,15] as well as clay minerals such as sodium-montmorillionite [16], bentonite [17], rectorite [18], montmorillonite [19], clay-polymer nanocomposites [20], starch-based nanocomposites [21] were used.

In this work, we have synthesized the ball clay-MnO_2 nanocomposite, which has been alternative choice to use as adsorbent for dye removal. The characterization of native ball clay and ball clay-MnO_2 nanocomposite were investigated using powder X-ray diffraction (Powder-XRD), Fourier transform infrared spectroscopy (FT-IR), scanning electron microscopy (SEM), transmission electron microscopy (TEM) and Brunauer, Emmet and Teller (BET) surface area.

EXPERIMENTAL

Preparation of ball clay-MnO_2 nanocomposite: Initially, the ball clay was washed several times with doubled distilled water to eliminate dust and other particle impurities. Then 15 g of clay was allowed to swell in 75 mL of water free alcohol and stirred to get uniform suspension for 3 h at room temperature. Then 15 g of manganese dioxide was dispersed into 75 mL water free alcohol. After that the diluted manganese dioxide was gradually dispersed into the clay suspension and stirred continuously for next 7 h at room temperature. Finally,

10 mL of alcohol was mixed with 1 mL of deionized water and added slowly in the clay-MnO_2 mixture. The stirring process was continued for further 6 h at room temperature. The final suspension was centrifuged and washed frequently with deionized water. The washed product was dried in a vacuum oven at 90 °C for 24 h and cooled to room temperature. The resultant product was stored in an air tightened container for further use and named as ball clay-MnO_2 nanocomposite.

Characterization study

X-ray diffraction study: X-ray diffraction (XRD) study was carried out on native ball clay and ball clay-MnO_2 nanocomposites to identify the crystalline phase. This technique was accomplished by BRUKER AXS D8 ADVANCE X- ray diffractometer with Cu anode and 1.5406 Å wavelength. By this instrument, the diffraction angle (2θ) could be measured from 3° to 135° and was operated by 40 kV voltage and 35 mA current.

FT-IR study: The FT-IR spectra was executed on native ball clay and ball clay-MnO_2 nanocomposites to identify the functional groups. The spectral range of the FT-IR was 4000 to 400 cm^{-1}. The FT-IR study was done by AVATAR 370 (Thermo Nicolet) spectrometer. In this technique, the powdered samples were mixed thoroughly with solid KBr and made thin pellets, which were used for FT-IR analysis.

Scanning electron microscopic study (SEM): The physical surface topography of the native ball clay and ball clay-MnO_2 nanocomposites were studied by scanning electron microscope. The surface of the both samples was studied by JSM – 6390LV, version 1.0 (JEOL) microscope. This system was accelerated at 20 kV of voltage and 10 mA of current.

Transmission electron microscopic study (TEM): Transmission electron microscope was used to identify the linkage of internal micro porous of the native ball clay and ball clay-MnO_2 nanocomposites. The micro pore uniformity of the both samples was imagined by JEM 2100 (JEOL) microscope. This system was operated at 200 kV of voltage. The alcohol (40 %) was used to dissolve the samples and allowed on the grid for TEM analysis. From the TEM images, the nanocomposite particles diameter was measured to determine its average size. Because of very tiny size of the nanocomposites, the selected area electron diffractometer (SAED) was studied on nanocomposites to attain the specific diffraction rings with d-values.

BET surface area study: Brunauer, Emmet and Teller (BET) method is based on the N_2 gas adsorption on the surface of the native ball clay and ball clay-MnO_2 nanocomposites. The BET was performed to calculate the surface area and the total pore volume of the samples. Before analysis, both samples were degassed at for 8 h at 120 °C. The N_2 gas adsorption was accompanied at 77 K using NOVA – 1000, version 3.70 instrument.

RESULTS AND DISCUSSION

X-Ray diffraction: The XRD patterns showed that the sharp peaks for the native ball clay and ball clay-MnO_2 nanocomposites, which were informed that the both samples were crystalline nature due to the presence of sharp peak [22]. The Figs. 1(a) and 1(b) indicated the XRD pattern of the native ball clay and ball clay-MnO_2 nanocomposites, respectively.

Ball clay indicated its specific peak at 2θ of 29.49°, which related to the d-spacing value of 3.02 Å. Some other peaks indicates that the presence of minerals in the ball clay. The XRD pattern of Ball clay-MnO_2 nanocomposites showed a peak at 2θ of 26.64°, which related to the d-spacing value of 3.34 Å. The specific peak of ball clay has been shifted from 29.49° to 26.64° in the ball clay-MnO_2 nanocomposites. The change in intensity of peak indicates that the internal structure of the native clay has been modified.

FT-IR study: The FT-IR spectra of the native ball clay and ball clay-MnO_2 nanocomposites showed in Fig. 2(a) and 2(b), respectively. In ball clay, the adsorption band near 3621 cm^{-1} is due to the – OH stretching vibration of water molecule [23], which was shifted to 3619 cm^{-1} in ball clay-MnO_2 nanocomposite. Both of them showed a band nearly at 1623 cm^{-1}, which related to the –OH bending vibration of water molecule. The –OH bending band at 911 cm^{-1} for ball clay and 914 cm^{-1} for ball clay-MnO_2 nanocomposite were assigned to Al-OH [24]. The band at 1021 cm^{-1} for ball clay, which was shifted to 1034 cm^{-1} in ball clay-MnO_2 nanocomposite and these bands were attributed to Si-O stretching vibration. Meanwhile, a band at 463 cm^{-1} for ball clay and at 469 cm^{-1} for ball clay-MnO_2 nanocomposite were found and assigned to Si-O-Si tetrahedral bending vibration. A new band in ball clay-MnO_2 nanocomposite was found at 539 cm^{-1}, which related to Si-O-Mn tetrahedral bending vibration. Also, a peak at 1420 cm^{-1} was found in native ball clay, which could be assigned to the carbonates and it was disappeared in ball clay-MnO_2 nanocomposite.

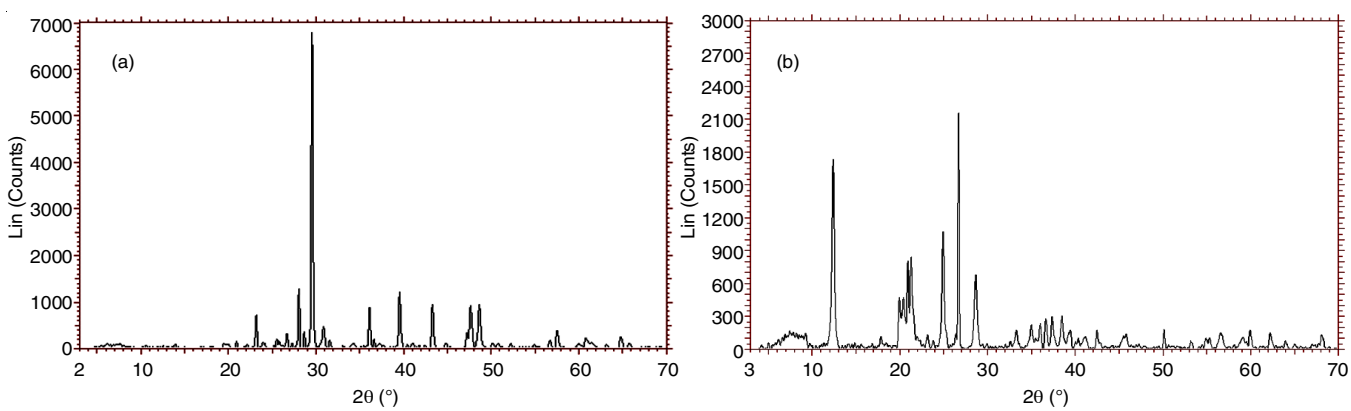

Fig. 1. (a) XRD pattern of native ball clay, (b) XRD pattern of ball clay-MnO_2 nanocomposites

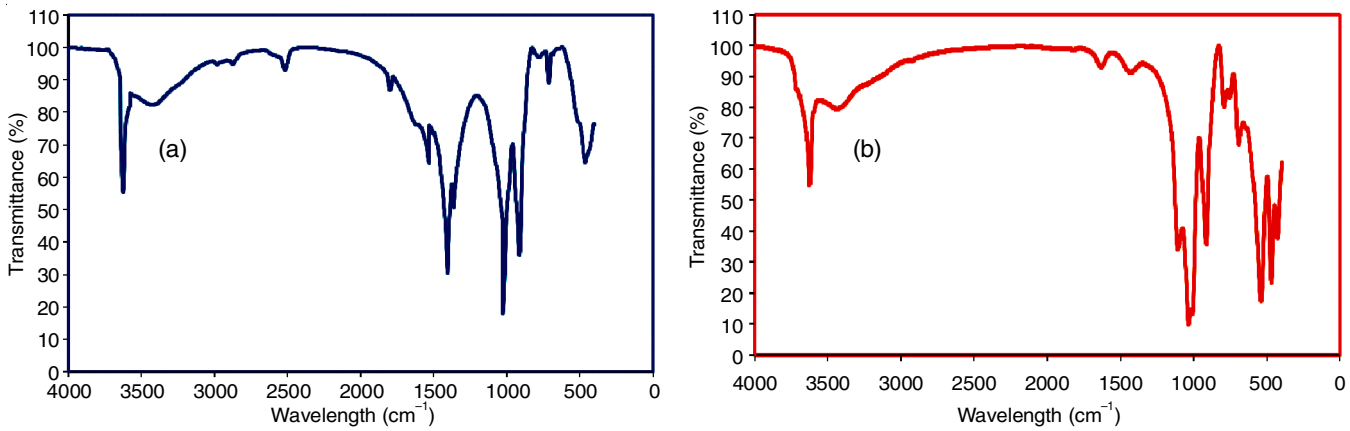

Fig. 2. (a) FT-IR spectra of native ball clay, (b) FT-IR spectra of ball clay-MnO_2 nanocomposites

Scanning electron microscope (SEM): The SEM images of the sample are presented in the Fig. 3(a) and 3(b) for native ball clay and Fig. 3(c) and 3(d) for Ball clay-MnO_2 nanocomposite, respectively. The surface changes noted in the ball clay-MnO_2 nanocomposite compared to native ball clay.

Ball clay was composed with different shapes and sizes of flakes along with damaged edges are noted. Some white deposits occur in the flakes, which might be few non-clay varieties present in the clay surface. The Ball clay-MnO_2 nanocomposite appeared with different shapes and sizes of the flakes and generally notable that the particle size (> 10 μm) was disappeared during the nanocomposite activation process. This would indicate that increasing the surface area of the nanocomposite compared with native ball clay. The nanocomposite surface looked to be more porous and uncovered.

Transmission electron microscopic study (TEM): Fig. 4(a) and 4(b) showed the TEM pictures of the native ball clay and Fig. 4(c), 4(d), 4(e) and 4(f) showed the TEM pictures of the ball clay-MnO_2 nanocomposite.

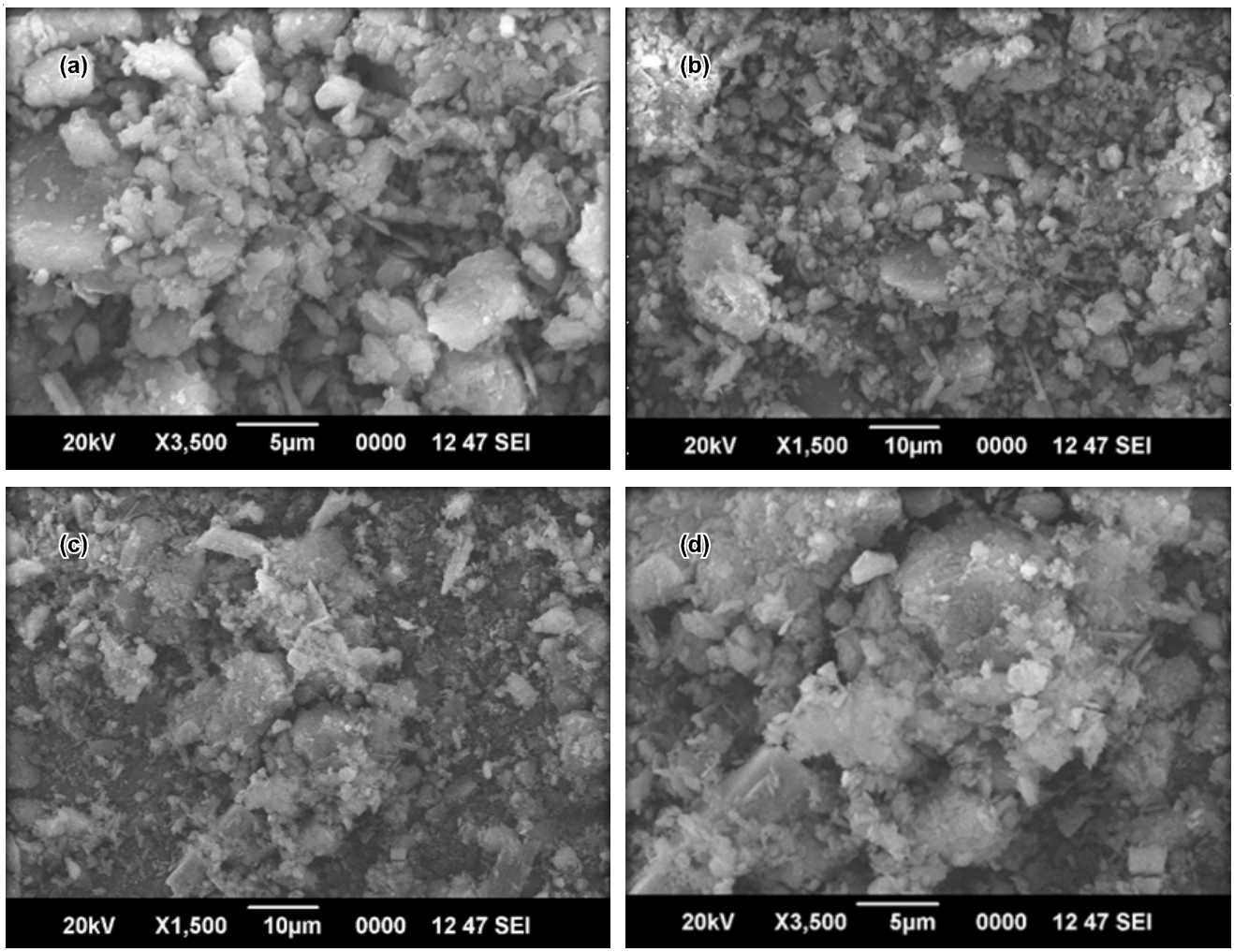

Fig. 3. (a) & (b) SEM images of native ball clay, (c) & (d) SEM images of ball clay-MnO_2 nanocomposites

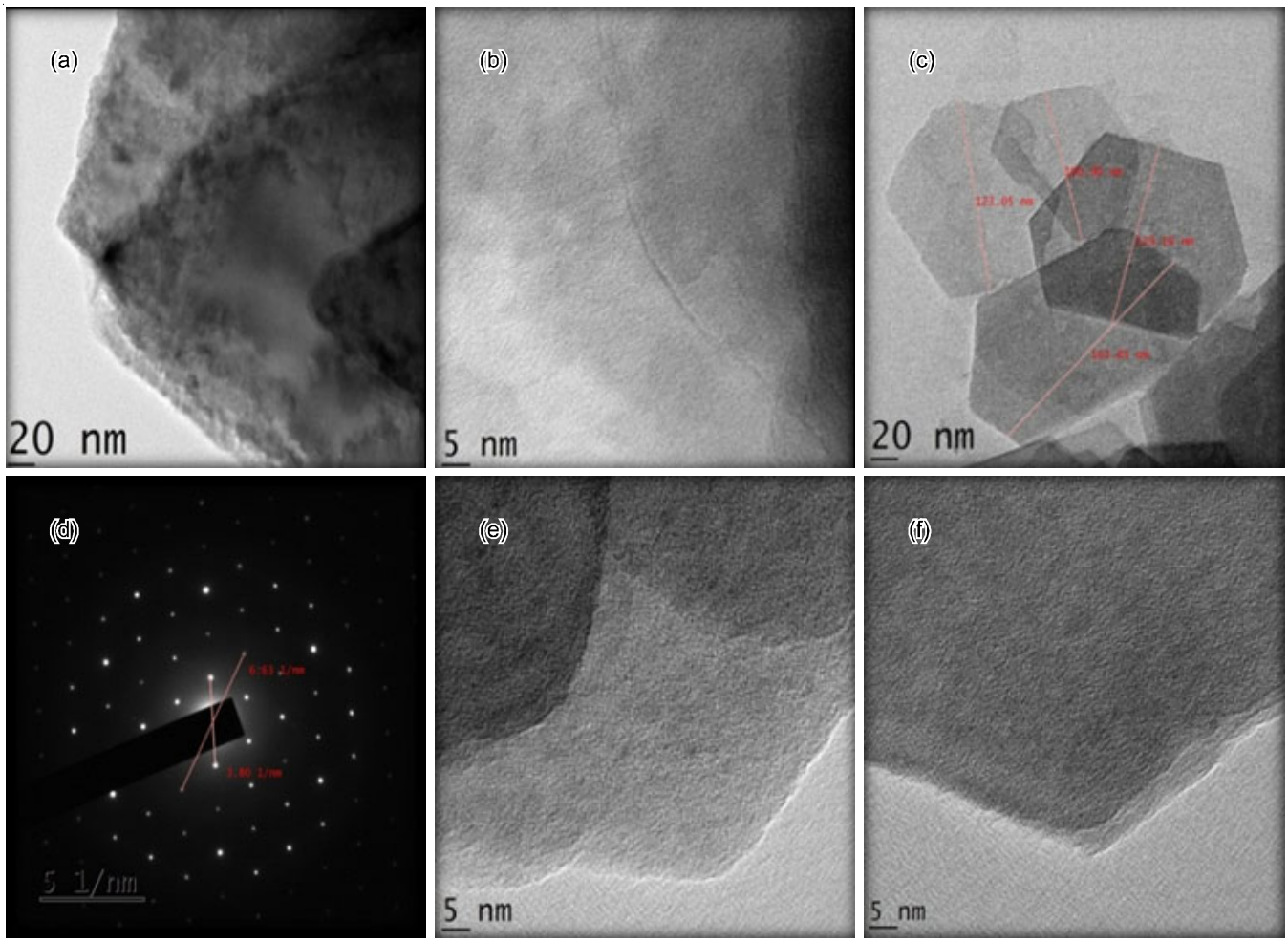

Fig. 4. (a) & (b) TEM images of native ball clay, (c), (d), (e) & (f) TEM images of ball clay-MnO_2 nanocomposites

From the Fig. 4(c), the dark spots might be belongs to the MnO_2 phase. The nanocomposite particles were randomly dispersed in the ball clay matrix. The size of the crystals varied from 100 to 170 nm. SAED pattern studied on ball clay-MnO_2 nanocomposite showed in Fig. 4(d) and the specific d-values measured (d_1 = 6.63 1/nm and d_2 = 3.80 1/nm).

Fig. 4(e) and 4(f) represents the development of MnO_2 nanocomposites into the native ball clay and the uniform size of the pores were identified undoubtedly.

BET surface area, pore volume and porosity: The nitrogen gas adsorption/desorption isotherms of the native ball clay and ball clay-MnO_2 nanocomposites were showed in Fig. 5(a) and 5(b), respectively. The native ball clay and ball clay-MnO_2 nanocomposites formed type IV isotherm belongs to IUPAC recommendation. The nature of this type of isotherm contains mesoporosity materials. This isotherm contains H_3 type of hysteresis loop according to IUPAC recommendation, which specifies split like pores. In native ball clay, the formation of monolayer started at low relative pressure (P/P_0) and continued till P/P_0 reaches at 0.45. But in ball clay-MnO_2 nanocomposite, the formation of monolayer started at low relative pressure (P/P0) and continued till P/P_0 reaches at 0.78.

From the formation of monolayer, this isotherm indicates that the pores were filled gradually also the amount of adsorption (cm^3/g) rises gradually. In ball clay-MnO_2 nanocomposite, the amount of adsorption increases suddenly from ~ 9 to 36 cm^3/g at P/P_0 ~1.0. This is due to the sudden filling of pores. The maximum adsorption was takes place ~ 17 cm^3/g at P/P_0 ~ 1.0 for native ball clay and ~ 36 cm^3/g at P/P_0 ~ 1.0 for ball clay-MnO_2 nanocomposite. The increase in maximum adsorption in ball clay-MnO_2 nanocomposite indicates the change in pore characteristics.

The pore and surface characteristics of native ball clay and ball clay-MnO_2 nanocomposites are listed in Table-1.

TABLE-1
PORE AND SURFACE CHARACTERISTICS

Sample	BJH pore diameter (nm)	Total pore volume (cm^3/g)	BET surface area (m^2/g)
Native ball clay	3.645	0.021	10.575
Ball clay-MnO_2 nanocomposite	1.566	0.051	11.529

BJH pore volume distribution curves with pore diameter of native ball clay and ball clay-MnO_2 nanocomposites showed in Fig. 5(c) and 5(d), respectively.

The increase in pore volume between the native ball clay and ball clay-MnO_2 nanocomposites were high. Also a small increase in pore volume of small pores of diameter, 5-10 nm and the large pores of diameter (15-35 nm) showed a high increase in pore volume.

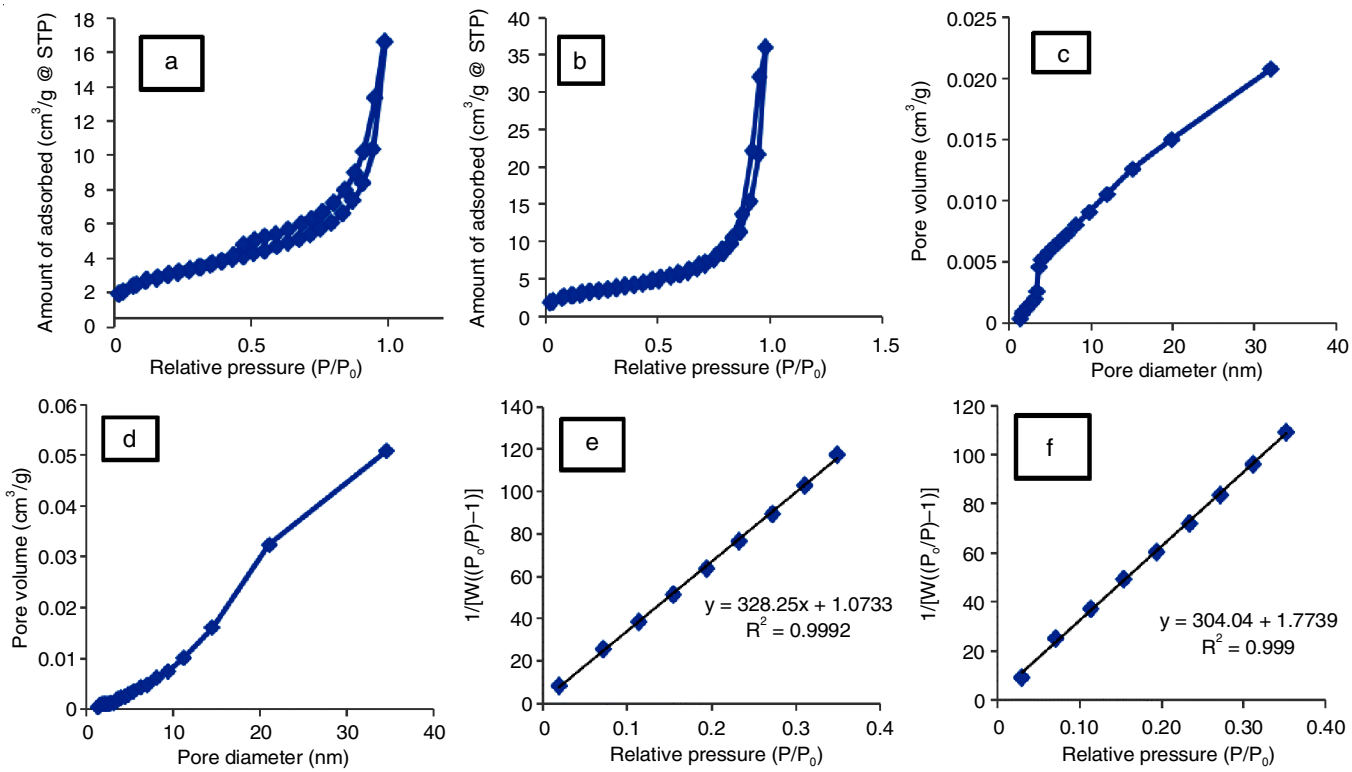

Fig. 5. (a) N_2 gas adsorption/desorption isotherms of the native ball clay, (b) N_2 gas adsorption/desorption isotherms of the ball clay-MnO_2 nanocomposites, (c) BJH pore volume distribution curves with pore diameter of the native ball clay, (d) BJH pore volume distribution curves with pore diameter of the ball clay-MnO_2 nanocomposites, (e) The BET plot of the native ball clay, (f) The BET plot of theball clay-MnO_2 nanocomposites

The BET plot was plotted between P/P_0 and 1 [W (P_0/P) – 1]. BET plot of native ball clay (Fig. 5(e)) and ball clay-MnO_2 nanocomposites (Fig. 5(f)) are linear.

Conclusion

This study discussed the preparation and characterization of ball clay-MnO_2 nanocomposites as adsorbent for dye removal. The XRD report established that ball clay-MnO_2 nanocomposite was crystalline in nature because of its sharp peak. The FT-IR study showed the formation of ball clay-MnO_2 nanocomposite, which confirmed by the different peak vibrations form the native ball clay. From the SEM images, the change in surface morphology of ball clay-MnO_2 nanocomposite specified the development of surface area. TEM images showed the size of the nanoparticles. BET surface area and total pore volume increased in ball clay-MnO_2 nanocomposites from native ball clay.

CONFLICT OF INTEREST

The authors declare that there is no conflict of interests regarding the publication of this article.

REFERENCES

1. G. Ciardelli, L. Corsi and M. Marcucci, *Resour. Conserv. Recycl.*, **31**, 189 (2000); https://doi.org/10.1016/S0921-3449(00)00079-3.
2. M. Muthukumar and N. Selvakumar, *Dyes Pigments*, **62**, 221 (2004); https://doi.org/10.1016/j.dyepig.2003.11.002.
3. N. Das, R. Vimala and P. Karthika, *Indian J. Biotechnol.*, **7**, 159 (2008).
4. S. Aoudj, A. Khelifa, N. Drouiche, M. Hecini and H. Hamitouche, *Chem. Eng. Process.: Process Intensif.*, **49**, 1176 (2010); https://doi.org/10.1016/j.cep.2010.08.019.
5. M.A. Gondal, C. Li, X. Chang, L. Sikong, Z.H. Yamani, Q. Zhou, F. Yang and Q. Lin, *J. Environ. Sci. Health-Part A*, **47**, 570 (2012); https://doi.org/10.1080/10934529.2012.650566.
6. L.W. Man, P. Kumar, T.T. Teng and K.L. Wasewar, *Desal. Water Treat.*, **40**, 260 (2012); https://doi.org/10.1080/19443994.2012.671257.
7. M. Sala and M.C. Gutiérrez-Bouzán, *Int. J. Photoenergy*, **Article ID 629103** (2012); https://doi.org/10.1155/2012/629103.
8. W. Chu, *Water Res.*, **35**, 3147(2001); https://doi.org/10.1016/S0043-1354(01)00015-X.
9. C. Namasivayam, M. Dinesh Kumar, K. Selvi, R. Ashruffunissa Begum, T. Vanathi and R.T. Yamuna, *Biomass Bioenergy*, **21**, 477 (2001); https://doi.org/10.1016/S0961-9534(01)00052-6.
10. F.C. Wu, R.L. Tseng and R.S. Juang, *Sep. Purif. Technol.*, **47**, 10 (2005); https://doi.org/10.1016/j.seppur.2005.03.013.
11. B.H. Hameed, A.L. Ahmad and K.N.A. Latiff, *Dyes Pigments*, **75**, 143 (2007); https://doi.org/10.1016/j.dyepig.2006.05.039.
12. J.X. Lin, S.L. Zhan, M.H. Fang, X.Q. Qian and H. Yang, *J. Environ. Manage.*, **87**, 193 (2008); https://doi.org/10.1016/j.jenvman.2007.01.001.
13. A.L. Cazetta, A.M.M. Vargas, E.M. Nogami, M.R. Guilherme, M.H. Kunita, A.C. Martins, T.L. Silva, J.C.G. Moraes and V.C. Almeida, *Chem. Eng. J.*, **174**, 117 (2011); https://doi.org/10.1016/j.cej.2011.08.058.
14. D. Schimmel, K.C. Fagnani, J.B.O. Dos Santos, M.A.S.D. Barros and E.A. Da Silva, *Braz. J. Chem. Eng.*, **27**, 289 (2010); https://doi.org/10.1590/S0104-66322010000200007.
15. A. Martins and N. Nunes, *J. Chem. Edu.*, **92**, 143 (2015); https://doi.org/10.1021/ed500055v.
16. O. Abollino, M. Aceto, M. Malandrino, C. Sarzanini and E. Mentasti, *Water Res.*, **37**, 1619 (2003); https://doi.org/10.1016/S0043-1354(02)00524-9.
17. E. Bulut, M.Özacar and I.A. Sengil, *Micropor. Mesopor. Mater.*, **115**, 234 (2008); https://doi.org/10.1016/j.micromeso.2008.01.039.

18. Y. Huang, X. Ma, G. Liang, Y. Yan and S. Wang, *Chem. Eng. J.*, **138**, 187 (2008); https://doi.org/10.1016/j.cej.2007.06.017.
19. B.A. Fil, M.T. Yilmaz, S. Bayar and M. Telkoca, *Braz. J. Chem. Eng.*, **31**, 171 (2014); https://doi.org/10.1590/S0104-66322014000100016.
20. E.I. Unuabonah and A. Taubert, *Appl. Clay Sci.*, **99**, 83 (2014); https://doi.org/10.1016/j.clay.2014.06.016.
21. R.F. Gomes, A.C.N. De Azevedo, A.G.B. Pereira, E.C. Muniz, A.R. Fajardo and F.H.A. Rodrigues, *J. Colloid Interface Sci.*, **454**, 200 (2015); https://doi.org/10.1016/j.jcis.2015.05.026.
22. D. Das, D.P. Samal, M. BC, *J. Chem. Eng. Process Technol.*, **06**, 248 (2015); https://doi.org/10.4172/2157-7048.1000248.
23. D.W. Cho, B.H. Jeon, C.M. Chon, Y. Kim, F.W. Schwartz, E.S. Lee and H. Song, *Chem. Eng. J.*, **200**, 654 (2012); https://doi.org/10.1016/j.cej.2012.06.126.
24. S. Ismadji, D.S. Tong, F.E.Soetaredjo, A.Ayucitra, W.H. Yu and C.H. Zhou, *Appl. Clay Sci.*, **119**, 146 (2016); https://doi.org/10.1016/j.clay.2015.08.022.